THE JOURNAL OF PHYSICAL CHEMISTRY B

Article

pubs.acs.org/JPCB

In-situ SAXS Study of Aqueous Clay Suspensions Submitted to Alternating Current Electric Fields

Erwan Paineau,*[,†] Ivan Dozov,[†] Adrian-Marie Philippe,[§] Isabelle Bihannic,[‡] Florian Meneau,[∥] Christophe Baravian,[§] Laurent J. Michot,[‡] and Patrick Davidson[†]

[†]Laboratoire de Physique des Solides, UMR 8502, Université Paris-Sud, Bâtiment 510, 91405 Orsay Cedex, France

[§]Laboratoire d'Energétique et de Mécanique Théorique et Appliquée, UMR 7563, Nancy University, BP 160, 54504 Vandoeuvre Cedex, France

[‡]Laboratoire Environnement et Minéralurgie, UMR 7569, Nancy University, BP 40, 54501 Vandoeuvre Cedex, France

[∥]Synchrotron SOLEIL, L'Orme des Merisiers, Saint-Aubin, BP 48, 91192 Gif-sur-Yvette Cedex, France

ABSTRACT: Aqueous colloidal suspensions of clay platelets display a sol/gel transition that is not yet understood. Depending on the nature of the clay, liquid-crystalline behavior may also be observed. For example, the suspensions of beidellite display a nematic phase whereas those of montmorillonite do not. Both beidellite and montmorillonite have a "TOT" structure but the structural electric charge is located in the tetrahedral layer for the former and in the octahedral layer for the latter. We built a setup to perform SAXS experiments on complex fluids submitted to an electric field *in situ*. We found that the fluid nematic phase of beidellite suspensions readily aligns in the field. However, the field had no influence on the gels, showing that the orientational degrees of freedom of the platelets are effectively frozen. Moreover, strong platelet alignment was induced by the field in the isotropic phase of both clays, in a similar way, regardless of their ability to form a nematic phase. This surprising result would suggest that the orientational degrees of freedom are not directly involved in the sol/gel transition. The ability to induce orientational order in the isotropic phase of clay suspensions can be exploited to prepare materials of controlled anisotropy.

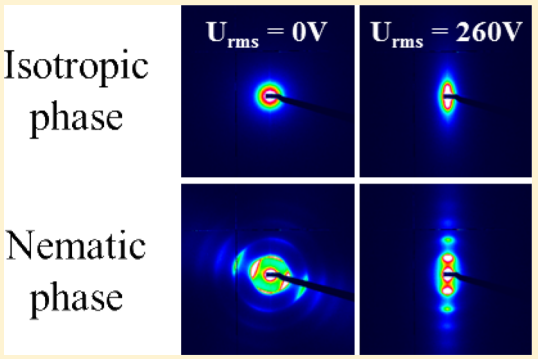

1. INTRODUCTION

Many clay minerals, called "swelling clays", spontaneously exfoliate in water. The colloidal suspensions thus obtained find, thanks to their original viscoelastic properties, widespread industrial applications in paints, cosmetics, oil-drilling, etc.[1,2] From a more fundamental point of view, aqueous clay suspensions have also recently raised much interest because they show a sol/gel transition, the origin of which is still largely debated,[3−17] and because they also sometimes show a nematic liquid-crystalline phase.[18−27] For example, the phase diagram of beidellite clay suspensions (Figure 1A) displays, upon increasing volume fraction, the usual isotropic liquid phase (I) where clay platelets are randomly oriented, a biphasic (isotropic/nematic) region, the nematic phase (N) where clay platelets cooperatively align in a common direction, and finally a gel state where platelet orientation and position are trapped.[25] However, in contrast, the phase diagram of montmorillonite clay suspensions (Figure 1B) does not display any liquid-crystalline phase but exhibits instead a direct transition from an isotropic phase to a birefringent gel state, suggesting that the I/N phase transition is simply "pre-empted" by the sol/gel transition.[14] The reasons why these two phase diagrams are so different still remain mysterious to date. It should be noted however that although beidellite and montmorillonite dioctahedral smectite clays both have a "TOT" structure, they differ by the location of their electrical charge that is in the tetrahedral layer for the former and in the octahedral layer for the latter. Accordingly, we recently highlighted differences in the strength of the repulsive potential between platelets in these clay suspensions.[28]

From a structural and static perspective, on the one hand, our previous investigations by small-angle X-ray scattering (SAXS) of these systems have shown that the organizations of the clay platelets in the fluid nematic phase and in the birefringent gel state are actually fairly similar, in terms of the structure factor that describes the liquid-like positional order.[28] On the other hand, these two systems may differ by their susceptibility to orientational order of the clay platelets. In this work, we examined by SAXS, at the microscopic scale, the influence of an ac electric field on the orientational order in the isotropic phase of beidellite and montmorillonite suspensions, for different concentrations and particle sizes. Our previous electro-optic study of beidellite isotropic suspensions suggests that the platelets align with their normal perpendicular to the field,

Received: June 30, 2012
Revised: October 29, 2012
Published: October 29, 2012

dx.doi.org/10.1021/jp3064728 | *J. Phys. Chem. B* 2012, 116, 13516−13524

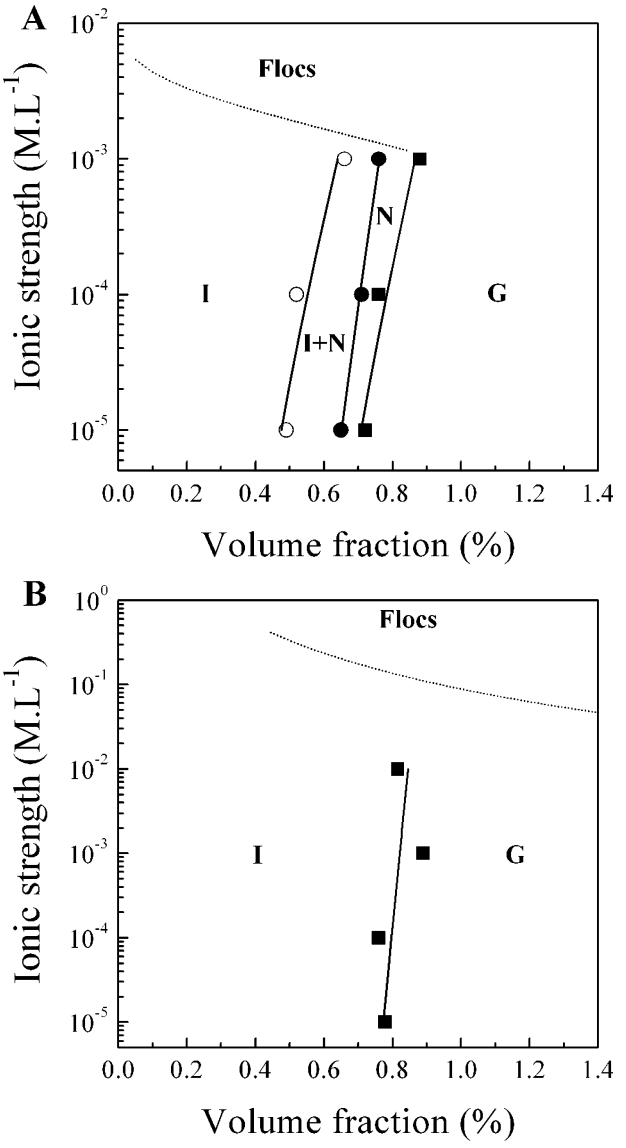

Figure 1. Examples of phase diagrams of the (A) SBId-1 beidellite (S3) and (B) SWy-2 montmorillonite (S2) clay aqueous suspensions after refs 25 and 14 (I = isotropic liquid, N = nematic liquid, G = gel).

resulting in uniaxial "antinematic" order.[29] Therefore, the aim of the present study was to examine the influence of the field on the orientational degrees of freedom of the platelets, at the microscopic scale, for both types of clay, in the isotropic, nematic, and gel phases.

For this purpose, we built a new cell that allows applying an ac electric field very easily to complex fluid samples held in sealed cylindrical glass capillary tubes commonly used for SAXS studies. We found that the nematic phase of beidellite clay suspensions is readily aligned by the electric field, as shown by its highly anisotropic SAXS pattern, but the field has no influence on the gels. Moreover, strong field-induced orientational order was observed in the isotropic phases of both montmorillonite and beidellite clay suspensions. Therefore, quite surprisingly, both types of clay qualitatively behave in the same way under field as concentration increases and the I/N and sol/gel transitions are approached.

2. MATERIALS AND METHODS

2.1. Sample Preparation. Natural dioctahedral smectites, a beidellite (SBId-1, Idaho) and a montmorillonite (SWy-2, Wyoming), were purchased from the Source Clays Mineral Repository of the Clay Mineral Society (Purdue University). Prior to use, raw samples were purified following a procedure previously established.[25] A 4 wt % clay suspension was exchanged three times in 1 mol·L^{-1} NaCl or LiCl solutions during 24 h. The suspension was then washed against Milli-Q water until the conductivity fell below 5 μS·m^{-1}. The suspensions were then poured into Imhoff cones and left to settle for 24 h. The bottom of the cone that contains miscellaneous impurities was discarded. The structural formulas of the purified smectites thus obtained are deduced from chemical analyses[25,30] and can be written as follows: $(Si_{7.27}Al_{0.73})(Al_{3.77}Fe^{3+}_{0.11}Mg_{0.21})O_{20}(OH)_4Na_{0.67}$ and $(Si_{7.74}Al_{0.26})(Al_{3.06}Fe^{3+}_{0.42}Fe^{2+}_{0.03}Mg_{0.48})O_{20}(OH)_4Na_{0.77}$, for SBId-1 and SWy-2, respectively. As all these samples are natural clays, isomorphous substitutions occur both in the tetrahedral (Si → Al, Fe) and octahedral layers (Al → Mg). In the case of beidellite, the electrical charge is mainly located in the tetrahedra whereas it is located in the octahedra for montmorillonites.

In addition to the purification process, a size fractionation procedure consisting in successive centrifugations was performed. The stock suspension was first centrifuged at 7000g during 90 min. The sediment was collected, rediluted in Milli-Q water, and will be referred to as "size 1 (S1)" hereafter. The same procedure was then applied after centrifugations at 17000g and 35000g, thus yielding "size 2 (S2)" and "size 3 (S3)" fractions. In the following, we will only focus on S2 and S3. The elementary particles of both smectites display disk-shape morphology as shown previously by transmission electron microscopy experiments.[28] The morphological parameters deduced from these observations coupled with SAXS measurements are reported in Table 1. All experimental details have been published elsewhere.[25,28]

Table 1. Average Diameter $\langle D\rangle$, Polydispersity $\sigma_D = (\langle D^2\rangle - \langle D^2\rangle)^{1/2}/(\langle D\rangle)$, Average Thickness $\langle t\rangle$, and Electrical Charge Density C of the Studied Clays

	SBId-1		SWy-2	
size	S2	S3	S2	S3
$\langle D\rangle$ (nm)	286	209	240	100
σ_D (%)	45	38	93	25
$\langle t\rangle$ (nm)	0.85	0.7	0.7	0.7
C (C·m^{-2})	−0.148	−0.168	−0.172	−0.172

Table 1 also summarizes the structural charges calculated by using the unit cell dimensions of the basal surface (0.45 nm^2) and the value of the cationic exchange capacity determined previously.[30] This method takes into account the charges induced by isomorphic substitutions as well as those resulting from broken bonds at the particle edges.

Batches of suspensions were prepared from the stock suspension for each size, by osmotic stress experiments at fixed ionic strengths (IS = 10^{-3} to 10^{-5} mol L^{-1}) in order to explore a wide clay concentration range, spanning from the isotropic sol to the gel phase. Clay suspensions were filled into regenerated cellulose dialysis tubes (Visking, MWCO = 14000 Da, Carl Roth GmbH) and put into a poly(ethylene glycol)

dx.doi.org/10.1021/jp3064728 | J. Phys. Chem. B 2012, 116, 13516−13524

(PEG 20000, Carl Roth GmbH) solution whose ionic strength was adjusted by adding the appropriate salt. Sample preparations are detailed elsewhere.[25] The clay volume fraction ϕ was determined at the end of the experiment by weight loss upon drying, taking into account the relative humidity according to the water adsorption isotherm of Na−saponite.[31]

2.2. Small Angle X-ray Scattering. SAXS measurements were performed at the SWING beamline of the synchrotron SOLEIL (Orsay, France) that was already described in detail.[32] Measurements were carried out using a fixed energy of 9 keV and a sample to detector distance of 7 m. The typical accessible range of scattering vector modulus q was 0.01−0.5 nm^{-1} ($q = 4\pi(\sin\theta)/\lambda$, where 2θ is the scattering angle and $\lambda = 0.138$ nm is the wavelength). The transverse dimensions of the incident X-ray beam were approximately 350 × 100 μm^2 in the horizontal and vertical directions, respectively. 2D scattering patterns were collected on an AVIEX CCD camera formed by four detectors and were corrected for water and glass scattering. Exposure times were typically around 100 ms −1 s. Samples of suspensions were transferred into borosilicate cylindrical Lindemann capillary tubes (diameter 1 mm, Mark-Rohrchen, Germany) and stored vertically after flame-sealing.

The curves of scattered intensity versus scattering vector modulus q were obtained either by angular integration of the data in the case of isotropic patterns or by integration within a narrow strip in the case of anisotropic patterns. Furthermore, the alignment of the suspensions that showed anisotropic patterns was assessed by extracting angular profiles of scattered intensity at constant q. This procedure provides the value, within relative error bars of about 10%, of the nematic order parameter, S_2, defined as $S_2 = (1/2)(3\cos^2\theta - 1)$ where θ is the angle of a platelet normal with the nematic director **n** and the brackets mean averaging over all platelets. By definition, S_2 takes values ranging between $-1/2$ and 1, with $S_2 = 0$ corresponding to the disordered isotropic phase. The spontaneous nematic order parameter is positive, $0 < S_2 < 1$ as the platelet normals point on average along the director **n**. However, negative values of S_2 may be induced by external fields, resulting in so-called "antinematic" order.[29] In this case, the platelet normals lie on average in the plane perpendicular to **n**, with isotropic angular in-plane distribution. In order to calculate S_2, we simply identify the orientational distribution function (odf) in real space with the angular profile in reciprocal space. This is justified here for the nematic phase because it shows a very strong short-range lamellar order that gives rise to rather sharp reflections so that each platelet "stack" oriented at some angle with the director scatters at precisely the same angle. Direct rigorous analytical calculations show that this approximation is also actually very good (within 10% error bars) in the case of the isotropic phase that has little short-range order. Then, we adopt the classical Maier−Saupe form for the orientational distribution function and calculate its second moment that is S_2.[33]

2.3. Description of the Electric-Field Setup. A pair of external electrodes made of aluminum foil, in direct contact with the outer wall of the capillary, was used to apply the electric field on the sample (Figure 2**A**). The electrodes are actually rings of foil, encircling completely the capillary, 2 mm apart along the capillary axis. A high-frequency (700 kHz) ac field was applied to the electrodes, with amplitude varying from 0 to 400 V. The sample holder is especially adapted to the thin-walled and fragile capillaries needed for the SAXS experiments. The electrodes are pressed onto the capillary protected by a cushion of soft foam to optimize the electrode/glass wall contact without damaging the capillary tube. The electric field penetrating into the suspension is moderately strong, up to about 100 V/mm rms value (corrected for the attenuation due to the screening by the mobile charges and the dielectric mismatch between suspension and capillary). Previous experimental studies and numerical simulations of the field penetration in the sample[29] confirmed that the field is parallel to the capillary axis, with highly uniform strength and orientation in the whole interelectrode area accessible for observation. This electric-field cell was fitted onto the experimental table of the Swing beamline, with the capillary tubes (and the electric field) held horizontal (Figure 2**B**). For each sample, two-dimensional SAXS patterns were recorded upon increasing and decreasing voltages U_{rms}, between 0 and 260 V. We report hereafter the experimental results as a function of the applied voltage. The rms value of the electric field E inside the sample was estimated from numerical simulations and frequency-dependent electric-birefringence experiments. Under the present experimental conditions, we obtained $E = 302 \times U_{rms}$ (V/m), giving $E = 7.8 \times 10^4$ V/m for the highest applied voltages, $U_{rms} = 260$ V.

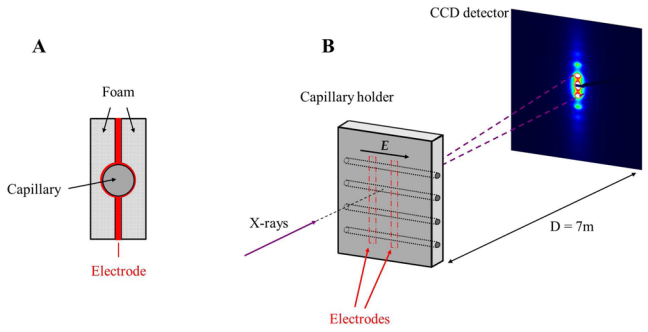

Figure 2. (A) Side view of the capillary holder. (B) Scattering geometry of the experiment.

3. RESULTS AND DISCUSSION

In zero-field, the SAXS pattern of the nematic phase of the beidellite clay suspensions reveals a randomly aligned polydomain texture (see the TOC figure). Indeed, the nematic director field is strongly distorted due to the absence of a well-defined surface anchoring on the inner wall of the capillary. The SAXS pattern varies rapidly upon translation of the sample in the beam, in terms of both direction and amplitude of anisotropy. Applying an ac electric field to this sample has a dramatic effect on its SAXS pattern (Figure 3A). Indeed, the pattern is very anisotropic because the clay particles align with their normal perpendicular to the applied field, thus confirming previous electro-optic studies.[29] Although the nematic texture (i.e., the distribution of nematic domains) is most probably still degenerated azimuthally with $\mathbf{n} \perp \mathbf{E}$, the domains for which the nematic director is almost perpendicular to the X-ray beam are the only ones that fulfill the scattering conditions and therefore contribute most to the SAXS pattern. Compared to the time scale of the SAXS experiment (of order of a minute), the alignment kinetics appears almost instantaneous. Moreover, once the nematic phase is fully aligned, its SAXS pattern does not depend on the field intensity, showing that the field-induced order is negligible compared to the strong spontaneous nematic order of the suspension. In fact, after switching the field off, the relaxation time of the SAXS pattern is of the order

dx.doi.org/10.1021/jp3064728 | J. Phys. Chem. B 2012, 116, 13516−13524

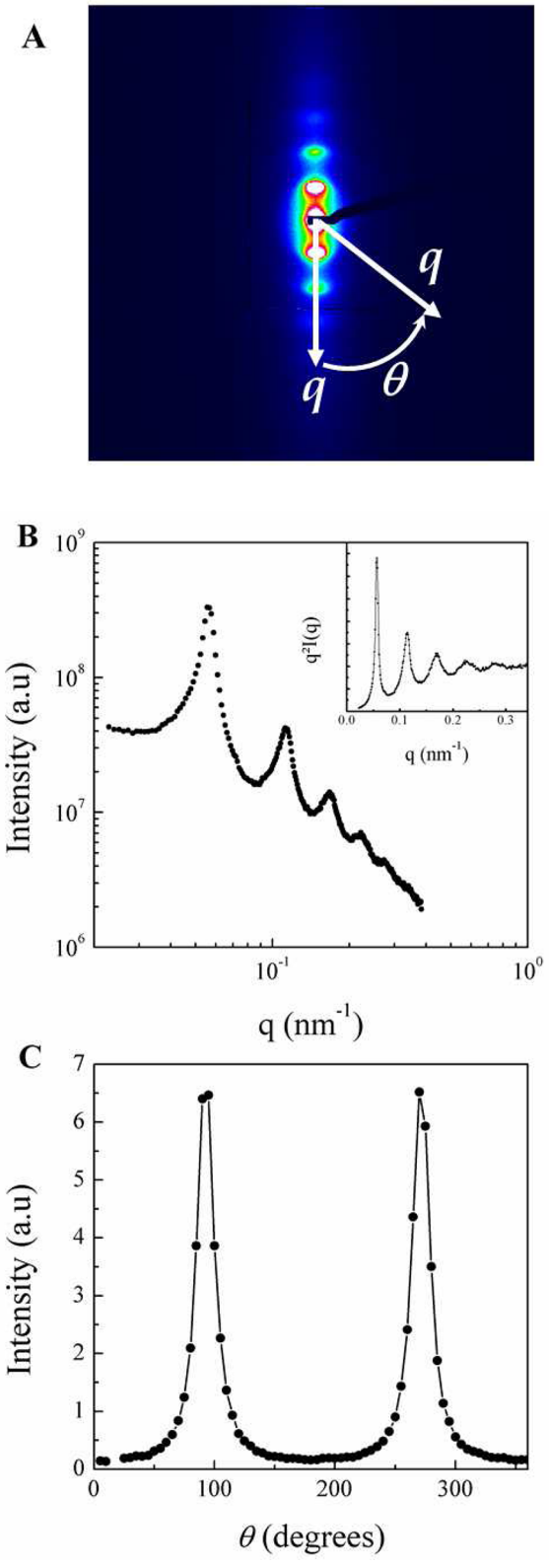

Figure 3. (A) SAXS pattern of a nematic sample of beidellite clay suspension (S3, IS = 10^{-4} M·L^{-1}, ϕ = 0.55%) aligned in an ac electric field (U_{rms} = 260 V). (B) $I(q)$ and (C) $I(\theta)$ curves.

of several hours, which is the time needed for the slow reorientation of the director back to the random multidomain texture.

Such an aligned pattern allows investigating the structure of the nematic phase in more detail. For example, the pattern displays a series of equidistant diffuse spots that arise from some lamellar short-range positional order of the beidellite clay sheets. Accordingly, a scan of the scattered intensity along the director, $I(q)$, reveals a large number of oscillations. By dividing $I(q)$ by the platelet form factor $P(q) \sim q^{-2}$ (Figure 3B), a quantity is obtained which is the best approximation of the structure factor $S(q)$ that can be reached in the present state of understanding of the scattering by such systems. Indeed, the difficulty here lies in decoupling the orientational and positional correlations of the clay platelets in a rigorous way, which remains an unsolved problem to date. In the absence of a better theoretical treatment, we will still use this approximation that allows comparing the SAXS patterns of different samples. Because the signal-to-noise ratio of an aligned sample is better than that of a powder sample, the data thus retrieved is of better quality. Nevertheless, no significant qualitative difference was observed between the $I(q)$ curves drawn from the SAXS patterns recorded with and without electric field, meaning that the field does not affect the positional short-range order of the platelets in the nematic phase. In addition, using well-documented procedures (see experimental part),[32,33] the nematic order parameter S_2 was drawn from an azimuthal scan of the scattered intensity along a circle at a fixed scattering vector modulus going through the diffuse spots (Figure 3C). The value obtained here, S_2 = 0.75 ± 0.05, confirms the very good alignment of the sample.

The isotropic phase of beidellite clay suspensions is also very sensitive to the application of an ac electric field (Figure 4A,B). As expected, its SAXS pattern is completely isotropic in zero-field. However, the pattern becomes anisotropic when the electric field is switched on as the clay particles align. In contrast with the nematic phase, the anisotropy of the SAXS pattern of the isotropic phase strongly depends on the field intensity. Moreover, the SAXS pattern fully recovers its isotropy

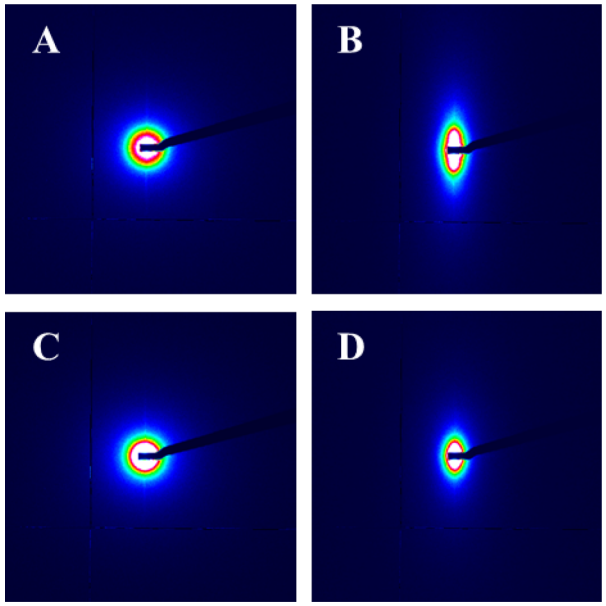

Figure 4. SAXS patterns of isotropic samples of (A, B) beidellite (S3, IS = 10^{-4} M·L^{-1}, ϕ = 0.31%) and (C, D) montmorillonite (S2, IS = 10^{-4} M·L^{-1}, ϕ = 0.27%) clay suspensions in zero-field (A, C) and submitted (B, D) to an ac electric field (U_{rms} = 260 V).

dx.doi.org/10.1021/jp3064728 | J. Phys. Chem. B 2012, 116, 13516−13524

when the electric field is suppressed and relaxation times vary between 1 ms and a few seconds, depending on the volume fraction and ionic strength. Such fast relaxation times are indeed expected for the Brownian rotational diffusion of the plate-like clay particles, in the absence of strong nematic-like interparticle correlations.

Although the aqueous suspensions of montmorillonite clay do not display any nematic phase at thermodynamic equilibrium, applying an ac electric field to the isotropic phase has, somewhat surprisingly, the same effects as those observed with the beidellite clay (Figure 4C,D). The SAXS pattern also becomes anisotropic, with orientation in the same direction, because the montmorillonite sheets also align with their normal perpendicular to the field. Moreover, the anisotropy of the pattern also depends on the field intensity. Therefore, both types of clay behave qualitatively in the same way when their isotropic phase is submitted to the field. Furthermore, it must be pointed out that the electric field has only a small influence on the structure factor of these suspensions (Figure 5). The position of the first maximum of

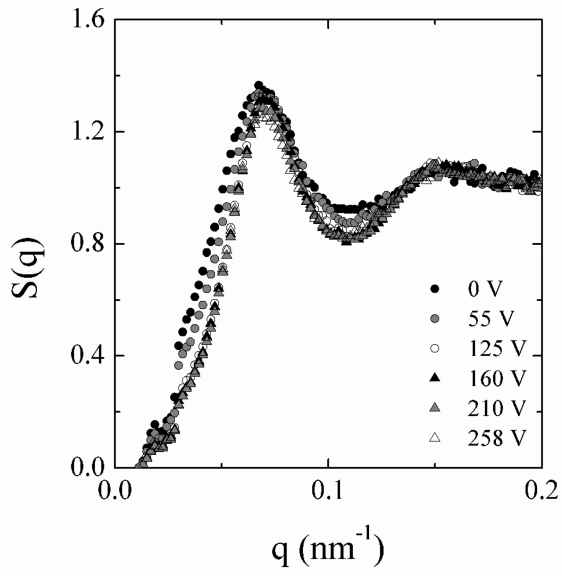

Figure 5. Influence of the applied voltage on the structure factor $S(q)$ for an isotropic suspension of beidellite (S3, IS = 10^{-4} M·L^{-1}, ϕ = 0.31%).

the structure factor does not depend on the voltage applied, which means that the field does not alter the average distance between platelets. However, the oscillations of the structure factor become sharper upon increasing voltage between 0 and 125 V. This could be due either to the field hampering the platelet positional fluctuations or to the fact that aligned samples frequently have crisper SAXS patterns than powder samples. This interesting observation should require a more specific study.

Using azimuthal scans of the scattered intensity, the field-induced nematic order parameter in the isotropic phase, $S_2(E)$, can be measured as a function of the applied field (Figure 6A). The dependence obtained always shows the same typical features. At low field intensity, $S_2(E)$ varies as E^2; then, an inflection point appears, and a plateau is reached at high field intensity, suggesting that the induced orientational order of the clay platelets saturates.

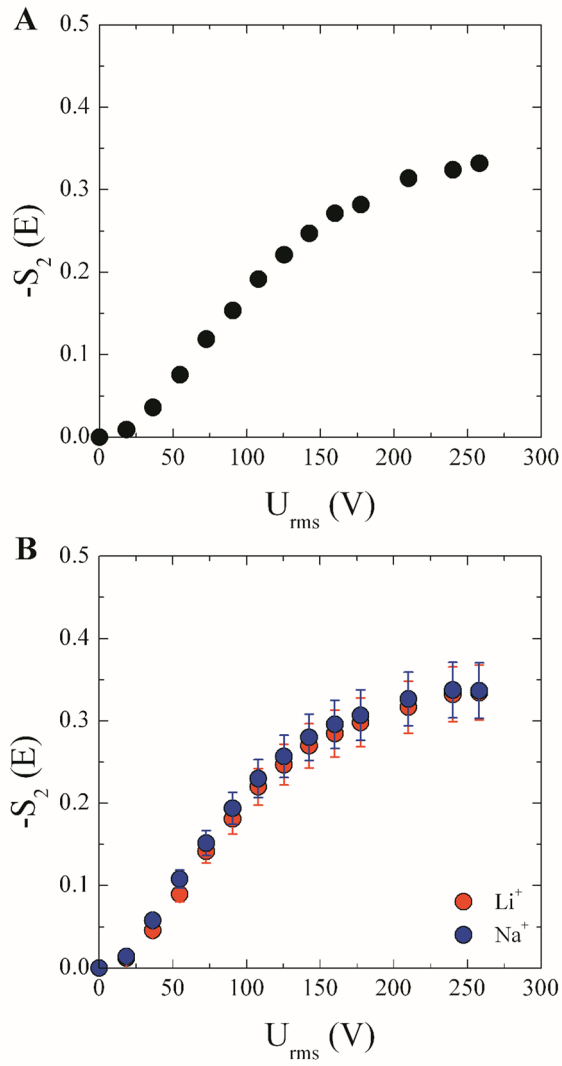

Figure 6. (A) Dependence of the field-induced orientational order parameter, S_2, on the applied voltage, U_{rms}, for an isotropic suspension of Na–beidellite (S3, IS = 10^{-4} M·L^{-1}, ϕ = 0.13%). (B) Comparison of the field-induced orientational orders for Li-beidellite and Na-beidellite (S3, IS = 10^{-4}, ϕ = 0.3%).

Although the electric field has a very strong effect on the orientation of the platelets in the isotropic phase for both types of clay, the field has no appreciable effect on the gel phase that is only slightly more concentrated than the isotropic one (data not shown). The orientational degrees of freedom of the platelets, probed in this experiment, thus appear frozen in the gel phase, like the translational ones. We therefore conclude that the electric torque acting on the platelets is too weak to overcome the mechanical effects of gelation.

We examined the influence of the nature of the counterions on the field-induced orientational order in the isotropic phase by comparing beidellite suspensions prepared with either Na^+ or Li^+ ions (Figure 6**B**). However, no difference was found, within our experimental precision, between the corresponding $S_2(E)$ curves and therefore no ionic-specificity effect of these monovalent cations was detected. Moreover, the influence of the ionic strength could not be investigated in much detail because no significant difference was found between samples prepared at IS = 10^{-4} M·L^{-1} and 10^{-5} M·L^{-1}, and because the

dx.doi.org/10.1021/jp3064728 | J. Phys. Chem. B 2012, 116, 13516–13524

electrical conductivity of samples prepared at IS = 10^{-3} M·L^{-1} was too large and the field penetration was therefore poor.

The influence of the volume fraction, ϕ, of the suspensions is illustrated by Figure 7 for both types of clay. All $S_2(E)$ curves

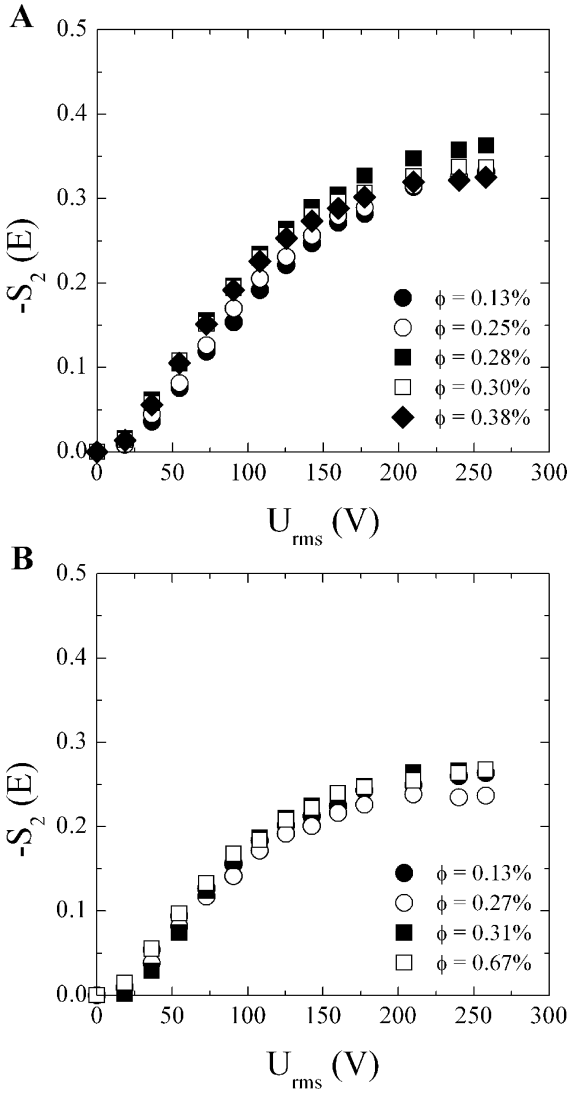

Figure 7. Influence of the volume fraction, ϕ, on the field-induced orientational order for (A) Na–beidellite (S3, IS = 10^{-4} M·L^{-1}) and (B) Na–montmorillonite (S2, IS = 10^{-4} M·L^{-1}) clay suspensions.

are quite similar, whatever the volume fraction. This clearly demonstrates that the field-induced alignment only results from the individual properties of noninteracting particles, as already suggested from our previous electro-optic investigations.

The influence of the nature of the clay platelets is illustrated by Figure 8A that draws a comparison between the two types of clay for the same platelet size and for suspensions of the same volume fraction and ionic strength. Although the respective curves are quite similar and fairly close together in the Kerr regime (i.e., at low fields), it seems that the field-induced orientational order at saturation is a bit stronger for the beidellite clay than for the montmorillonite clay. This reminds that the beidellite suspensions can form a nematic phase whereas the montmorillonite suspensions cannot, which underlines the larger orientational susceptibility of beidellite.

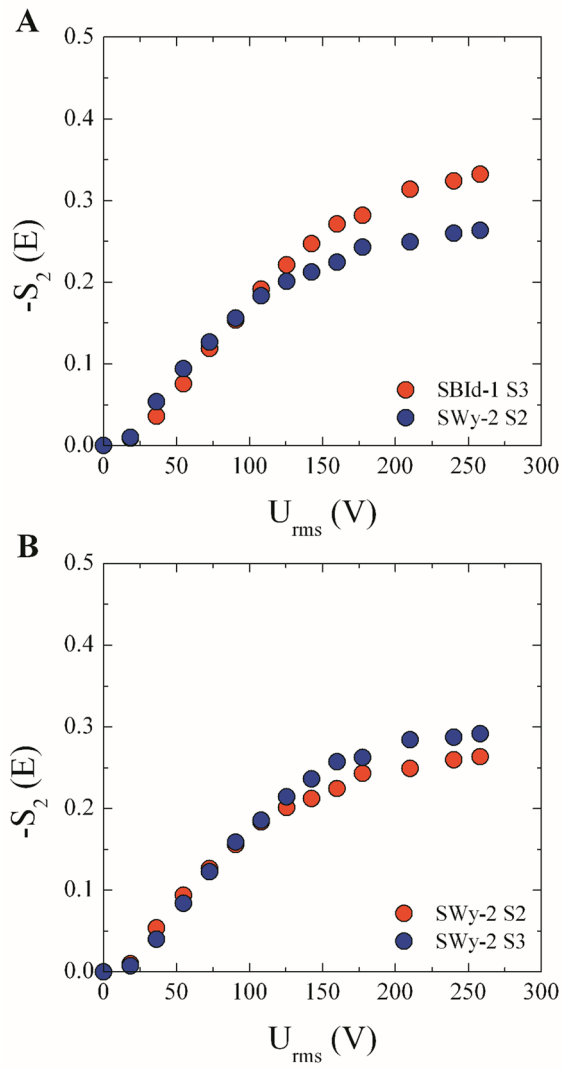

Figure 8. Evolution of the field-induced orientational order as a function of the applied voltage with (A) the clay nature (beidellite S3 and montmorillonite S2) and (B) the platelet size (montmorillonite S2 and S3) for clay suspensions (IS = 10^{-4} M·L^{-1}, ϕ = 0.13%).

Finally, the influence of the platelet size is shown in Figure 8B where the behaviors of montmorillonite platelets of two very different sizes are compared. Obviously, the experimental curves are very close together, within error bars. Therefore, the platelet size, in the range 100–250 nm, has a negligible influence, probably because the particle anisotropy is too large in this range.

Our in situ SAXS investigations of clay suspensions submitted to an ac electric field confirm and extend our previous electro-optic studies of the field-induced orientation of beidellite platelets in the isotropic phase. Qualitatively speaking, the clay sheets align with their normal perpendicular to the field, resulting in perpendicular orientation of the director of nematic domains and in "antinematic" induced order in the isotropic phase. Our findings agree with previous studies of similar colloidal systems of plate-like particles submitted to electric fields such as epoxy-montmorillonite composites, niobate nanosheets, and gibbsite platelets.[34,35] However, we noticed some quantitative differences between the SAXS and electro-optic measurements (Figure 9A) that are discussed below.

dx.doi.org/10.1021/jp3064728 | J. Phys. Chem. B 2012, 116, 13516–13524

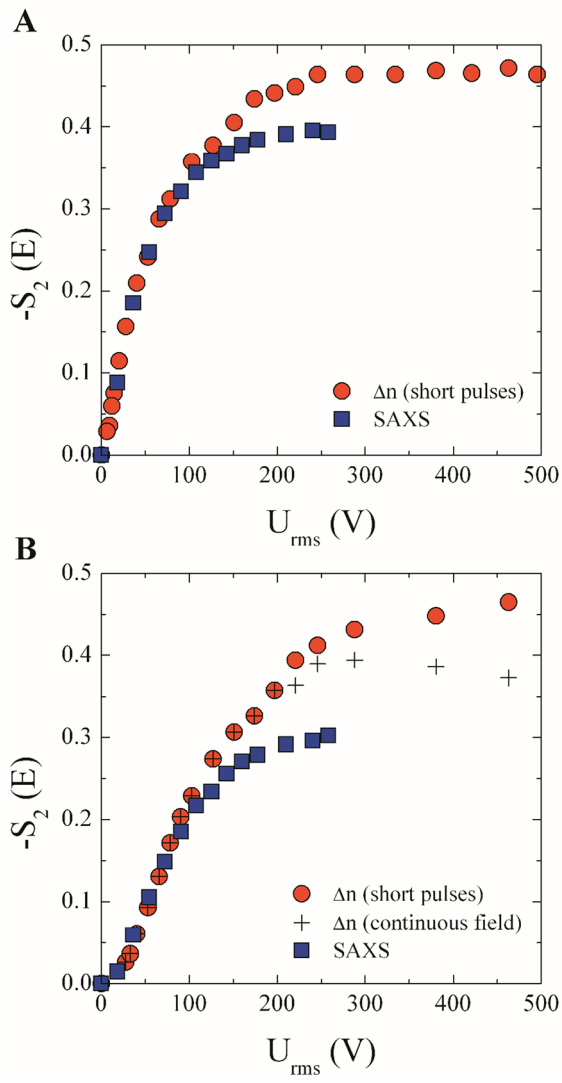

Figure 9. Field-induced orientational order measured in time-resolved (red circles) and steady-state (crosses) birefringence Δn and SAXS (blue squares) experiments: (A) Li–beidellite (S2, IS = 10^{-5} M·L^{-1}, ϕ = 0.43%); (B) Li–montmorillonite (S3, IS = 10^{-4} M·L^{-1}, ϕ = 0.28%).

In order to compare SAXS and optical experiments, we measured the field-induced birefringence of the isotropic phase in the same samples, using the same sample holder and electric-field setup. A peak voltage up to 700 V (sinusoidal waveform, f = 700 kHz) was applied to the electrodes, using an additional homemade ferrite transformer.[28] In a first series of experiments, the field was applied in short bursts (τ < 100 ms) taking advantage of the time-resolved birefringence response. Typical results are shown in Figure 9**A**. The curve of induced order measured by time-resolved birefringence, $S_2(E)_{\Delta n}$, shows the behavior theoretically expected, with a fast increase of the orientational order with increasing field, followed by a saturation to $S_2(E)_{sat} \approx -0.5$. At low fields, the SAXS results, $S_2(E)_{SAXS}$, overlap with the $S_2(E)_{\Delta n}$ curve, showing good agreement between the two measurement techniques. At high fields, however, the SAXS results saturate to rather low $S_2(E)_{sat}$ values, typically in the range −0.3 to −0.4, that cannot be explained by the models presently available.

The discrepancy between the SAXS and the birefringence results at high fields may possibly be due to the heating of the sample by the electric field. Indeed, the dissipated power density due to the Joule heating of the sample is P = σE^2, where $\sigma \approx 2 \times 10^{-3}$ S/m is the conductivity of the clay suspensions. At the highest field applied here, $E = 7.8 \times 10^4$ V/m, P = 12 W/cm^3, resulting in a heating rate of about 3K/s if we neglect heat losses. Although the direct effect of heating on the order parameter is rather weak (S_2 varies slowly with the temperature in lyotropic systems), the induced thermal convection leads to spurious flows. Consequently, the heated sample is no longer a single-domain and the measured macroscopic average of the order parameter is lower than its microscopic saturated value $S_2(E)_{sat} = -0.5$.

In the time-resolved electro-optic experiment, the heating is minimized by using short (<100 ms) pulses applied at a low repetition rate (<1 Hz). Because of the longer exposure times required for SAXS, time-resolved experiments at this rate could not be performed and the heating-related artifacts could not be avoided. We examined the influence of the Joule heating in a second series of electro-optic experiments, performed in steady-state regime under continuously applied ac field (Figure 9B). For E > 100 V/mm, the steady-state results lie below the pulsed-field ones and saturate to a significantly lower value, $S_2(E)_{sat} \approx -0.4$. Qualitatively, this confirms that the Joule heating is the main reason why lower values of the order parameter are measured at high fields in the steady-state SAXS experiments. However, the SAXS measurements are still significantly lower than those of the steady-state birefringence, showing a stronger effect of heating in the SAXS experiment than in the birefringence one.

To understand this observation, we need to take into account that, in the SAXS case, the intense X-ray beam, focused on the capillary, makes an important additional disturbance of the sample. First, the beam also contributes to the heating of the sample, with a power density $P_X = kI_X/V_X$, where $I_X \approx 2$ mW is the estimated total power of the X-ray beam focused on the sample, $k \approx 0.5$ is the X-ray absorption coefficient, and V_X = 0.35 × 0.1 × 1 mm^3 is the volume exposed to the beam. Neglecting thermal losses, we obtain $P_X \approx 30$ W/cm^3 and a maximal heating rate of about 7 K/s, which is clearly larger than the Joule heating. Moreover, the beam-heating is *local*, occurring only in the area exposed to the beam. This induces strong convective flows and a much more effective flow-induced disorientation in the examined area. Second, although we did not observe any permanent radiation damage to the samples, the ionization of the suspension under the intense X-ray radiation locally increases the charge carrier density. This further enhances the local Joule heating and also locally affects the electrical properties of the fluid, such as its conductivity. Therefore, the field distribution inside the sample may no longer remain uniform and may show lower field intensity in the high-conductivity region under study.

In spite of intense recent experimental work, the gelation of clay suspensions still remains a poorly understood phenomenon. Most studies published to date, such as rheological investigations, focus on how gelation freezes the translational degrees of freedom of the clay platelets. Our experiments show that the particles in clay gels do not align at all when submitted to an electric field, which demonstrates that gelation affects not only the translational degrees of freedom but also the orientational ones. The electric torque exerted by the field on the particles can be calculated for our experimental conditions. It is indeed well established that the main interaction with the electric field for a charged colloidal particle is due to the huge

dx.doi.org/10.1021/jp3064728 | J. Phys. Chem. B 2012, 116, 13516–13524

polarization of the counterion atmosphere around the particle.[36] For the strongly anisometric clay sheets (D/t ≈ 300) examined here, the torque exerted by the field on the particle is: $\Gamma^{p}(\theta) = -(1/2)\varepsilon_0\varepsilon_w E^2 V^p (4D/\pi t) \sin 2\theta$ where $\varepsilon_w \approx 80$ is the dielectric constant of the solvent (water), V_p is the platelet volume, and θ is the angle between the platelet normal and the field. For beidellite S3, under the maximum field $E = 7.8 \times 10^4$ V/m, we obtain: $\Gamma^{p}(\theta) = -4.5(\sin 2\theta)kT$(where k is the Boltzmann constant). In the isotropic phase, the individual reorientation of each particle under this strong torque leads to: $\langle \cos^2\theta \rangle \approx 0$, i.e., to almost-perfect field-induced antinematic order with $S_2 \approx -1/2$ and director **n** parallel to **E**. In the nematic phase, the strong interactions between the particles result in the alignment of the nematic director perpendicular to the field, leading only to a very minor effect on the already high nematic order parameter $S_2 \approx 0.8$. Comparing the mechanical torque acting on a platelet in the gel phase with the electric one would be very interesting. However, in the absence of a microscopic description of the gel structure, it is highly difficult to obtain a value for the mechanical torque from macroscopic data such as the yield stress or the storage modulus. At this stage, we can merely state that the gelation creates a mechanical torque larger than about $5kT$ on the platelets.

In addition, we did not detect any significant qualitative difference in the orientational susceptibility of the isotropic phase between both types of clay in the vicinity of the sol/gel transition. This unexpected result would suggest that the translational degrees of freedom are indeed those directly involved in the sol/gel transition whereas the orientational ones would only be frozen as a result of the gelation process. In this case, orientational locking of the particles would only result from the "cage" formation brought about by gelation. However, this point should be studied in more detail by increasing the number of samples of concentrations spanning the region of the sol/gel transition.

4. CONCLUSION

In summary, our new setup allows applying ac electric fields easily to complex fluids in capillaries and performing X-ray scattering experiments *in situ*. The orientational order of anisotropic nanoparticles submitted to an electric field can thus be probed directly at the microscopic scale. We studied the colloidal suspensions of two types of clay that differ by the location of their structural electric charge, either in the tetrahedral layer or in the octahedral one. The liquid-crystalline nematic phase, observed with only one of them, namely beidellite, is readily aligned by the electric field, with its director oriented perpendicularly to the field because of the negative anisotropy of electric permittivity. Moreover, the electric field induced strong "antinematic" orientational order of the clay platelets in the isotropic phase. The orientational order, $S_2(E)$, follows a quadratic dependence with the field at low field and saturates, at high fields, to large values that are only limited by Joule heating and X-ray irradiation effects. The fact that both types of clay show similar behaviors in the field is somewhat surprising since the nematic phase (i.e., spontaneous orientational order) is only observed with beidellite suspensions. Then, it seems that, upon increasing volume fraction, the sol/gel transition suddenly occurs in montmorillonite suspensions due to a mechanism that would not directly involve platelet orientation.

From a more applied point of view, we recently showed how the orientational order of the clay platelets induced by the electric field in the isotropic phase can be frozen within hydrogels by polymerizing a water-soluble organic monomer under field.[37] Thus, materials of controlled anisotropy may easily be produced for barrier or optical applications.[38−41]

AUTHOR INFORMATION

Corresponding Author

*E-mail: erwan-nicolas.paineau@u-psud.fr.

Notes

The authors declare no competing financial interest.

ACKNOWLEDGMENTS

The authors gratefully acknowledge the ANR (Agence Nationale de la Recherche, "programme blanc" ANISO) for financial support and the Synchrotron SOLEIL for the award of beamtime 20100180. I.D. acknowledges financial support from Institut National Polytechnique de Lorraine (Nancy).

REFERENCES

(1) Odom, I. E. *Philos. Trans. R. Soc. London, Ser. A: Math. Phys. Eng. Sci.* **1984**, *311*, 391−409.
(2) Harvey, C. C.; Lagaly, G. In *Handbook of Clay Science*; Bergaya, F., Theng, B. G., Lagaly, G., Eds.; Elsevier: New York, 2006; Chapter 10.1.
(3) Broughton, G.; Squires, L. *J. Phys. Chem.* **1936**, *40*, 1041−1053.
(4) Van Olphen, H. *Discuss. Faraday Soc.* **1951**, *11*, 82−84.
(5) Norrish, K. *Discuss. Faraday Soc.* **1954**, *18*, 120−134.
(6) Callaghan, I. C. O., R.H. *Faraday Discuss.* **1974**, *57*, 110−118.
(7) Ramsay, J. D. F. *J. Colloid Interface Sci.* **1986**, *109*, 441−447.
(8) Mourchid, A.; Delville, A.; Lambard, J.; Lecolier, E.; Levitz, P. *Langmuir* **1995**, *11*, 1942−1950.
(9) Mourchid, A.; Lecolier, E.; Van Damme, H.; Levitz, P. *Langmuir* **1998**, *14*, 4718−4723.
(10) Knaebel, A.; Bellour, M.; Munch, J. P.; Viasnoff, V.; Lequeux, F.; Harden, J. L. *Europhys. Lett.* **2000**, *52*, 73−79.
(11) Abou, B.; Bonn, D.; Meunier, J. *Phys. Rev. E* **2001**, *64*, 021510.
(12) Bonn, D.; Kellay, H.; Tanaka, H.; Wegdam, G.; Meunier, J. *Langmuir* **1999**, *15*, 7534−7536.
(13) Jabbari-Farouji, S.; Eiser, E.; Wegdam, G. H.; Bonn, D. *J. Phys.: Condens. Matter* **2004**, *16*, L471−L477.
(14) Michot, L. J.; Bihannic, I.; Porsch, K.; Maddi, S.; Baravian, C.; Mougel, J.; Levitz, P. *Langmuir* **2004**, *20*, 10829−10837.
(15) Martin, C.; Pignon, F.; Piau, J. M.; Magnin, A.; Lindner, P.; Cabane, B. *Phys. Rev. E* **2002**, *66*, 021401.
(16) Martin, C.; Pignon, F.; Magnin, A.; Meireles, M.; Lelievre, V.; Lindner, P.; Cabane, B. *Langmuir* **2006**, *22*, 4065−4075.
(17) Cocard, S.; Tassin, J. F.; Nicolai, T. *J. Rheol.* **2000**, *44*, 585−594.
(18) Langmuir, I. *J. Chem. Phys.* **1938**, *6*, 873−896.
(19) Gabriel, J. C. P.; Sanchez, C.; Davidson, P. *J. Phys. Chem.* **1996**, *100*, 11139−11143.
(20) Lemaire, B. J.; Panine, P.; Gabriel, J. C. P.; Davidson, P. *Europhys. Lett.* **2002**, *59*, 55−61.
(21) DiMasi, E.; Fossum, J. O.; Gog, T.; Venkataraman, C. *Phys. Rev. E* **2001**, *64*, 061704.
(22) Michot, L. J.; Bihannic, I.; Maddi, S.; Funari, S. S.; Baravian, C.; Levitz, P.; Davidson, P. *Proc. Natl. Acad. Sci. U.S.A.* **2006**, *103*, 16101−16104.
(23) Michot, L. J.; Bihannic, I.; Maddi, S.; Baravian, C.; Levitz, P.; Davidson, P. *Langmuir* **2008**, *24*, 3127−3139.
(24) Michot, L. J.; Baravian, C.; Bihannic, I.; Maddi, S.; Moyne, C.; Duval, J. F. L.; Levitz, P.; Davidson, P. *Langmuir* **2009**, *25*, 127−139.
(25) Paineau, E.; Antonova, K.; Baravian, C.; Bihannic, I.; Davidson, P.; Dozov, I.; Imperor-Clerc, M.; Levitz, P.; Madsen, A.; Meneau, F.; et al. *J. Phys. Chem. B* **2009**, *113*, 15858−15869.
(26) Fonseca, D. M.; Meheust, Y.; Fossum, J. O.; Knudsen, K. D.; Parmar, K. P. S. *Phys. Rev. E* **2009**, *79*, 021402.

(27) Hemmen, H.; Ringdal, N. I.; De Azevedo, E. N.; Engelsberg, M.; Hansen, E. L.; Meheust, Y.; Fossum, J. O.; Knudsen, K. D. *Langmuir* **2009**, *25*, 12507−12515.
(28) Paineau, E.; Bihannic, I.; Baravian, C.; Philippe, A. M.; Davidson, P.; Levitz, P.; Funari, S. S.; Rochas, C.; Michot, L. J. *Langmuir* **2011**, *27*, 5562−5573.
(29) Dozov, I.; Paineau, E.; Davidson, P.; Antonova, K.; Baravian, C.; Bihannic, I.; Michot, L. J. *J. Phys. Chem. B* **2011**, *115*, 7751−7765.
(30) Vantelon, D.; Montarges-Pelletier, E.; Michot, L. J.; Briois, V.; Pelletier, M.; Thomas, F. *Phys. Chem. Miner.* **2003**, *30*, 44−53.
(31) Michot, L. J.; Bihannic, I.; Pelletier, M.; Rinnert, E.; Robert, J. L. *Am. Mineral.* **2005**, *90*, 166−172.
(32) Bihannic, I.; Baravian, C.; Duval, J. F. L.; Paineau, E.; Meneau, F.; Levitz, P.; de Silva, J. P.; Davidson, P.; Michot, L. J. *J. Phys. Chem. B* **2010**, *114*, 16347−16355.
(33) van der Beek, D.; Petukhov, A. V.; Davidson, P.; Ferre, J.; Jamet, J. P.; Wensink, H. H.; Vroege, G. J.; Bras, W.; Lekkerkerker, H. N. W. *Phys. Rev. E* **2006**, *73*, 041402.
(34) Koerner, H.; Jacobs, D.; Tomlin, D. W.; Busbee, J. D.; Vaia, R. D. *Adv. Mater.* **2004**, *16*, 297−302.
(35) Nakato, T.; Nakamura, K.; Shimada, Y.; Shido, Y.; Houryu, T.; Iimura, Y.; Miyata, H. *J. Phys. Chem. C* **2011**, *115*, 8934−8939.
(36) O'Konski, C. T. *J. Phys. Chem.* **1960**, *64*, 605−619.
(37) Paineau, E.; Dozov, I.; Bihannic, I.; Baravian, C.; Krapf, M. E. M.; Philippe, A. M.; Rouzière, S.; Michot, L. J.; Davidson, P. *ACS Appl. Mater. Interfaces* **2012**, *4*, 4296−4301.
(38) Tetsuka, H.; Ebina, T.; Tsunoda, T.; Nanjo, H.; Mizukami, F. *Nanotechnology* **2007**, *18*, 355701.
(39) Itoh, T.; Ishii, R.; Ebina, T.; Hanaoka, T.; Ikeda, T.; Urabe, Y.; Fukushima, Y.; Mizukami, F. *Biotechnol. Bioeng.* **2007**, *97*, 200−205.
(40) Priolo, M. A.; Gamboa, D.; Holder, K. M.; Grunlan, J. C. *Nano Lett.* **2010**, *10*, 4970−4974.
(41) Ebina, T.; Mizukami, F. *Adv. Mater.* **2007**, *19*, 2450−2453.